Oxidation of Metals, Vol. 24, Nos. 3/4, 1985

Deformation and Cracking Behavior of Protective Oxide Scales on Heat-Resistant Steels under Tensile Strain

M. Schütze*

Received March 21, 1985

The deformation and cracking behavior of oxide scales formed in air on four heat-resistant steels and on nickel 99.6 have been studied in constant-extension-rate tests at 800°C. The strain rates in the experiments ranged between 10^{-6} and 10^{-9} s^{-1}. Acoustic emission (AE) was used as an instrument for detecting the beginning of scale cracking. Additionally, metallographic, SEM, and microprobe investigations were performed which supported the results from the AE measurements. The strain-to-cracking of the scales did not exceed 0.5% except when lateral growth effects in the oxide scales occurred, leading to critical strains of up to nearly 2.5%. Also the crack distribution in the scales was measured. The deformation and cracking behavior of the scales investigated could be explained by model like considerations.

KEY WORDS: heat-resistant steels; nickel; oxide-scale cracking; acoustic emission; constant-extension-rate tests.

INTRODUCTION

The formation of protective oxide scales on heat-resistant steels is a prerequisite for the use of these materials in aggressive environments. The protective effect of these scales is only guaranteed as long as the scales can keep their integrity. Under practical conditions oxide scales have to stand various attacks of a chemical and mechanical nature which may lead to a temporary or final loss of the protective effect. Therefore, in recent years increasing interest has focussed on the behavior of protective oxide scales

*Dechema-Institut, D-6000 Frankfurt/M. 97, West Germany.

0030-7700/85/1000-0199$04.50/0

under near-service conditions. The results of previous research in this field are summarized in a volume comprising the papers of a conference on the technical meaning of oxide scales on high-temperature materials.[1]

Under service conditions high-temperature structural components always undergo a certain deformation by creep resulting from the various stresses in an operating plant. These stresses are transferred into the surface oxide scales, which may be chemically stable in the service environment, but which are susceptible to cracking under stress. As noted in the above-mentioned volume and other publications,[2-8] there are some excellent models describing the conditions which lead to scale-crack formation. Also, some experimental results are quoted which support these models, but generally there is a great lack of data, especially for the technically most important oxide scales on heat-resistant materials.

From the technical point of view, two main questions arise concerning data of protective oxide scales on metals during deformation:

1. What is the critical strain or strain rate for the beginning of oxide-scale cracking? (Strains and strain rates of components can be calculated in design and traced in service quite easily.)
2. Does scale cracking inevitably lead to subsequent increased internal corrosion and thus eventually to premature failure of a component, or is the protective effect of the scale restored by crack healing in such short times that enhanced corrosion does not occur?

The more conservative approach would be not to allow any oxide-scale cracking during service, which unfortunately is impossible. Therefore, investigations should concentrate not only on cracking data of scales but also on the ability of these scales to heal and maintain their protective capability. The present paper presents cracking data of oxide scales on four widely used heat-resistant steels and on pure nickel which are subjected to tensile straining. A following paper will deal with the healing behavior of these scales.

DATA FROM THE LITERATURE

The oxides encountered in protective scales on heat-resistant materials may be Al_2O_3, Cr_2O_3, Cr–Mn–spinel, NiO, and SiO_2. For these oxides only very few data are found in the literature concerning the cracking behavior of oxide scales on metals under tensile stress. In particular there are very few data measured at service temperatures.

First, a perusal of bulk-oxide data may be helpful. There are a large number of publications dealing with the high-temperature deformation behavior of bulk Al_2O_3.[9-18] Most of these data indicate that one cannot expect considerable plastic deformation below 1200°C unless impurities

form a glassy phase at grain boundaries enabling some plastic deformation to occur by grain-boundary sliding.[17] At very slow strain rates ($10^{-10}\,s^{-1}$ and below), there may also be a limited contribution to deformation by diffusional creep at temperatures below 1200°C.[18] In ref. 19 a transition temperature from brittle to "ductile" behavior is given for Al_2O_3 which amounts to about 1000°C.

Below the transition temperature neither diffusional creep nor the contribution by dislocation glide are sufficient to cause extensive plastic deformation. Extensive plastic deformation by dislocation glide cannot be expected since the number of the primary slip systems in the oxide is less than five[19] (at least five independent systems are necessary for plastic deformation by glide processes[20]). Below the transition temperature local stresses are relieved by the formation of cracks rather than by the activation of secondary slip systems.[21] All in all, there is no evidence for considerable plastic deformation of pure bulk Al_2O_3 at temperatures of 1000°C and below where the operation temperatures for most of the heat-resistant steels lie. This is supported by a fracture-mechanism map of Al_2O_3 showing that cracking occurs without macroscopic plasticity below 1000°C.[22]

Few data are found for Cr_2O_3, NiO, and SiO_2, and none for Cr-Mn-spinel. Plastic deformation of Cr_2O_3 by creep has been observed at temperatures of 1200°C and above.[23] Diffusional creep has been found for NiO at temperatures of 1000°C and above,[24-26] and for SiO_2 there is some evidence of creep at 825°C.[27] One may be inclined to assume that the transition temperature decreases in this sequence, but except for SiO_2 no data appeared indicating considerable plastic deformation under tensile stresses at temperatures below 1000°C.

The deformation behavior of growing oxide scales may be different from bulk oxide for various reasons. There is, e.g., a vacancy gradient within the scale which may play a role in the case of diffusional creep. Increased plasticity of Cr_2O_3 scales on Cr in oxidation studies at 800–1100°C has been attributed to an increased vacancy concentration at low p_{O_2}.[28,29] Further effects may come from internal growth processes in the scales, from doping elements, different grain sizes, different inherent mechanically relevant defect sizes, etc. In particular, the size and distribution of defects like microcracks, flaws, and voids will influence the cracking behavior of the scale based on fracture mechanics.

An answer to the question for the mechanical behavior of oxide scales on metals can be given only by investigating scales under "natural" conditions. This implies that the scales are at service temperature, that they have grown on the metal, and that the growth processes can still occur. The experiments reported here include these conditions, and the experimental technique used is described in the following section.

EXPERIMENTAL PROCEDURE

Tests were performed with four heat-resistant steels: a ferritic 18 Cr-0.8 Al-1.5 Si steel (in the following: 18 Cr steel), a ferritic 18 Cr-1.1 Al-1.5 Si-0.12 Ce steel (in the following: 18 Cr-Ce steel), a ferritic 24 Cr-1.4 Al-1.0 Si steel (in the following: 24 Cr steel) and an austenitic 32 Ni-20 Cr steel known as Alloy 800. Some additional tests also included Ni 99.6. The composition of the materials is given in Table I.

The oxide scales formed on the steels investigated in air at the testing temperature of 800°C consist of a sequence (from the outside to the inside) Cr-Mn-oxide, Cr_2O_3, Al_2O_3 for the ferritic steels; and of a sequence Cr-Mn-oxide, Cr_2O_3, SiO_2 for the austenitic Alloy 800.[30] Al_2O_3 is by far the thickest partial layer in the scale on the 24 Cr steel and also after longer testing times on the 18 Cr steel. The thickest partial layer in the scale on Alloy 800 is found to be Cr_2O_3 in most cases.

Cylindrical, tensile-test specimens were prepared from hot-rolled bars of the alloys and of nickel, and the gauge lengths were finished by abrading (final dimensions: gauge length 40 mm, diameter 8 mm, thread M 16). In order to measure the critical values for oxide-scale cracking on these materials, constant strain-rate tensile tests were performed at 800°C in air with these specimens, which were subjected to simultaneous oxidation and deformation. At this temperature the investigated steels still exhibit sufficient strength for long-term service. The strain rates, $\dot{\varepsilon}_o$, ranged between 10^{-6} and 10^{-9} s^{-1}. Constant strain-rate tests were chosen since they allow the measurement of critical strains as well as of critical strain rates. In parallel with these tensile tests, specimens were also kept in the same furnaces without straining to reveal differences in oxidation behavior between strained and unstrained specimens. The tests were terminated after different times so

Table I. Chemical Composition of the Alloys Tested (wt.%)

	C	P	Si	Ti	Cr	Mn	Fe	Ni	Al	S	Cu	Ce
18 Cr steel	0.066	0.018	1.48		18.19	0.50	r[a]		0.80	0.006		
18 Cr-Ce steel	0.12	0.048	1.50		18.7	1.00	r		1.14	0.012		0.12
24 Cr steel	0.088	0.033	0.97		24.12	0.57	r		1.41	0.003		
Alloy 800	0.070		0.37	0.44	20.99	0.99	r	33.50	0.26	0.005	0.60	
Ni 99.6	0.018		0.05			0.10	0.07	99.62		0.003	0.02	

[a] r = remainder.

that for each applied strain rate a number of specimens with different testing times (and different strains) were available for further investigations.

The test rigs used, which also allow tests in different corrosive gas atmospheres and which have been built at Dechema-Institut, and the computerized data acquisition and testing machine control are described elsewhere.[31,32]

A main feature of the tensile tests was the use of the acoustic emission (AE) technique in order to reveal cracking of the oxide scales during the experiments. Dunegan/Endevco equipment was used (3000 series) which enabled the total number of AE events to be recorded. In all cases the signals were filtered with a lower limit of 100 kHz and a higher limit of 350 kHz, for the band-pass. The transmission of the acoustic waves from the specimen in the hot zone of the furnace to the AE transducer at the outside occurred via a Pt-waveguide, which was pressed to the nondeformed part of the specimen by a clamp. A schematic of the test arrangement inside the gas-tight chamber of the furnace is shown in Fig. 1.

After the tests the surfaces of the specimens were investigated with a stereo-microscope and by scanning electron microscopy (SEM). Sections through the specimens were prepared and investigated by optical microscopy and electron probe microanalysis (EPMA). Oxide-scale cracking has been identified by the following applied methods.

1. *Surface investigations after the tests.* These provide optical evidence of cracks in the oxide scales. Usually, however, it cannot be distinguished whether cracks have formed at temperatrue or by cooling down after the tests. In the present investigations it had been found that scale cracks only appeared on deformed specimens after certain strains. Therefore, it is assumed that scale cracking is not primarily effected by cooling down but by deformation of the specimens at temperature.

2. *Investigation of metallographic sections after the tests.* These investigations allow the course of internal corrosion to be followed. If an increase of depth of internal corrosion is observed in deformed specimens, but not in nondeformed specimens at the same testing time, it can be concluded that scale cracking by deformation must have occurred before. However, it may also be the case that increased internal corrosion after scale cracking is prevented by instant crack healing.[39] Therefore, results from these investigations will be used only as a confirmation for scale cracking for cases where the protective effect is not quickly restored by crack healing. Furthermore, investigations of this kind can provide information about the healing capabilities of the oxide scales.

3. *Acoustic-emission technique.* Sudden, strong increases of the acoustic-event rate could be attributed to the formation of oxide scale cracks.[30,39-41] Contrary to the other methods, the acoustic-emission technique allows an

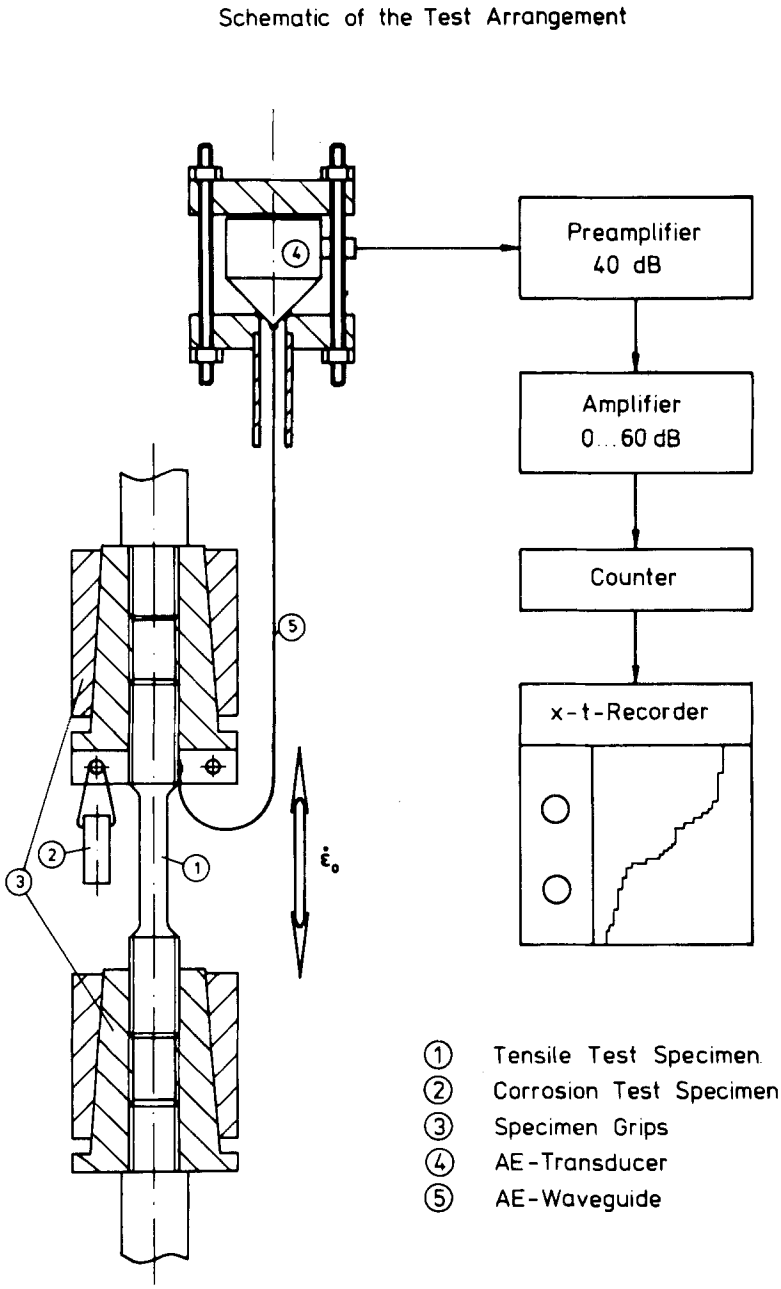

Fig. 1. Schematic of the test arrangement.

in-situ registration of oxide-scale cracking processes. It should, however, be emphasized that using this technique without comparing its results to results from other methods of investigation, e.g., surface and metallographic examinations, one may be going astray.

Beside information about scale cracking, the investigations also provided data about scale morphology, lateral oxide growth, and scale thickness.

RESULTS

The following sections are largely concerned with the results from the heat-resistant steels. A few additional results come from the investigations of Ni 99.6.

Surface appearance of the oxide scales

The most remarkable result of these investigations was that the surface of nondeformed specimens of the 18 Cr steel and of the 24 Cr steel showed

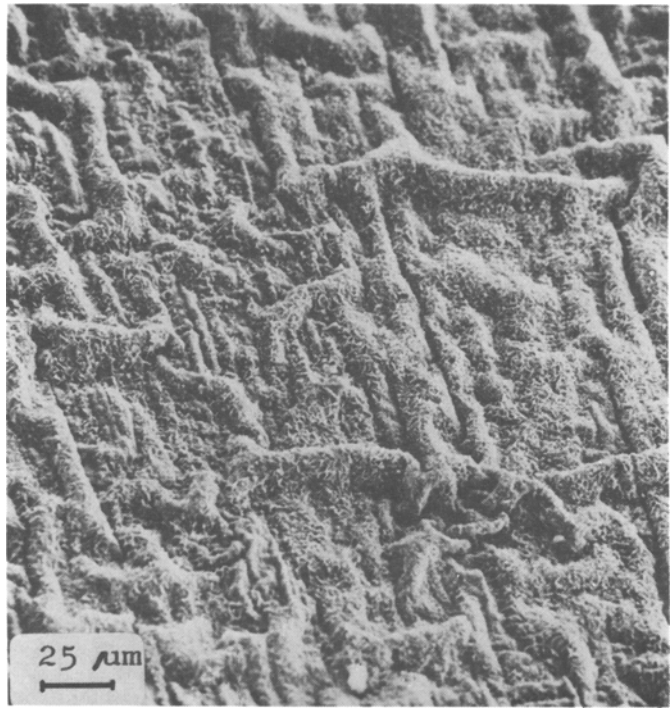

Fig. 2. Oxide wrinkles on a nondeformed specimen of the 18 Cr steel after 100 hr at 1000°C in air.

oxide scale wrinkles which were often arranged perpendicular to each other; see Fig. 2. The scales on the 18 Cr-Ce steel, on Alloy 800, and on Ni 99.6 did not exhibit any wrinkles for nondeformed specimens.

When the specimens of the two ferritic steels without Ce addition had been strained, again oxide wrinkles had formed, but these were aligned parallel to the tensile axis; see Figs. 3 and 4. Their dimensions seemed to increase with increasing time and strain, respectively. No wrinkles were found on the strained specimens of ferritic steel with Ce addition, on Alloy 800, Fig. 5, or on Ni 99.6. In the literature, the formation of wrinkles has been attributed to a lateral growth of the oxide scales occurring simultaneously with thickness growth as a result of the formation of new oxide within the scales.[28,29,33-36]

On strained specimens, oxide cracks were found after certain testing times and strains, respectively (see e.g., Figs. 3, 4, and 5). This is valid for all investigated materials with the exception of the ferritic steel with Ce addition. On the latter, a smooth oxidized surface was always encountered, even at a strain rate of $10^{-6}\,s^{-1}$ and a total strain of 28.8%. (As it turned

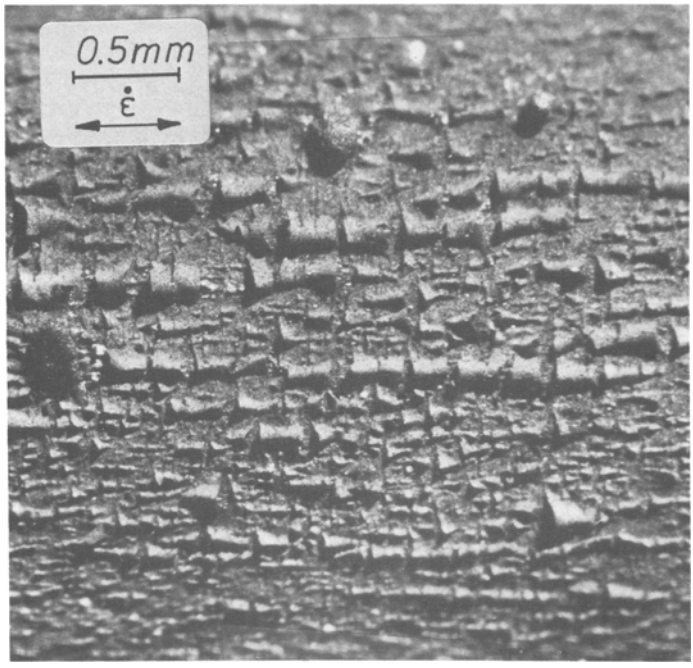

Fig. 3. Surface appearance of a deformed specimen of the 18 Cr steel after a test at 800°C (strain rate about $10^{-6}\,s^{-1}$, test duration 100 hr, strain 28.8%).

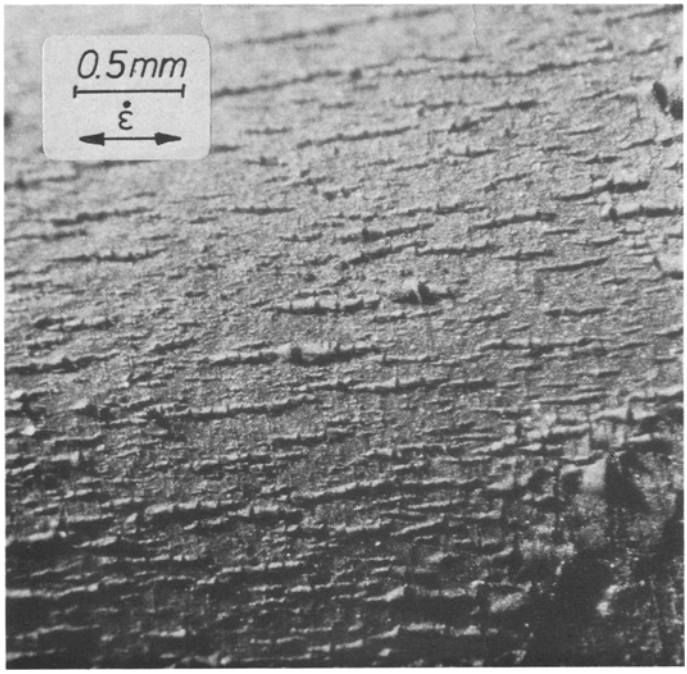

Fig. 4. Surface appearance of a deformed specimen of the 24 Cr steel after a test at 800°C (strain rate $10^{-6}\,s^{-1}$).

out from the results of the AE measurements, scale cracking had occurred several times, but rapid crack healing had made the original scale cracks disappear.)

For specimens with conspicuous scale cracks, an evaluation of the crack distribution in the oxide scales was performed. This led to average values of the distance between the cracks, l_R, which are shown in Fig. 6 as a function of the applied strain rate. The values are from the specimens with the highest strains attained in the tests at the respective strain rate. The upper line represents the values for the NiO scale on nickel; the values of the scales on the ferritic steels, which form scales consisting predominantly of Al_2O_3, lead to the line in the middle. The third line includes values of the scales on Ni80Cr20, where pure chromia had formed,[37] and on Alloy 800, which forms a scale in which Cr_2O_3 is the thickest partial layer.

Extent of Lateral Growth of the Oxide Scales

The formation of new oxide within the scale leads to compressive stresses. If the oxide scale is strained at the same time, a stress balance has

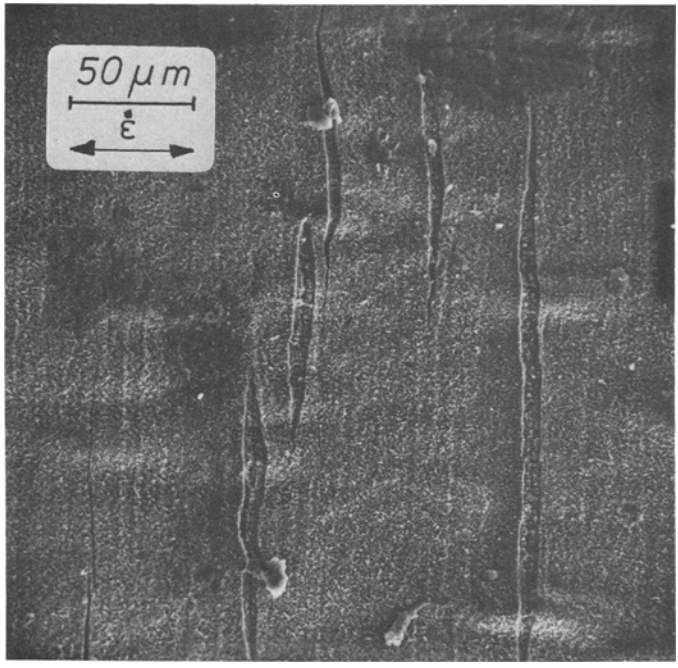

Fig. 5. Surface appearance of a deformed specimen of Alloy 800 after a test at 800°C (strain rate $10^{-6}\,s^{-1}$).

to be made between the compressive contribution form lateral growth and the tensile stresses arising from straining the specimen.

The scales on two of the investigated ferritic steels had shown considerable lateral growth. This was very marked on the 18 Cr steel, whereas it was not so extreme on the 24 Cr steel. In a former paper,[38] a method is described which gives the possibility of estimating the amount of lateral scale growth in the case of oxide-wrinkle formation. This method, by which the lateral increase of oxide "length" is measured in metallographic cross-sections, had been applied to the scales on the 18 Cr steel. An example of the appearance of such a scale in a metallographic cross-section is shown in Fig. 7. On the 24 Cr steel lateral scale growth was not marked enough for a quantitative estimation by this method. The results are shown in Figs. 8–10. The term $(U_{ox} - U_o)/U_o$ represents the amount of lateral scale growth, ε_{lat}, in the circumferential direction of the specimens (which is assumed to be equal in the longitudinal direction). $(U_{met} - U_o)/U_o$ stands for the decrease of the metal circumference by elongation of the specimen (uniform deformation assumed). In these graphs a comparison is made between the

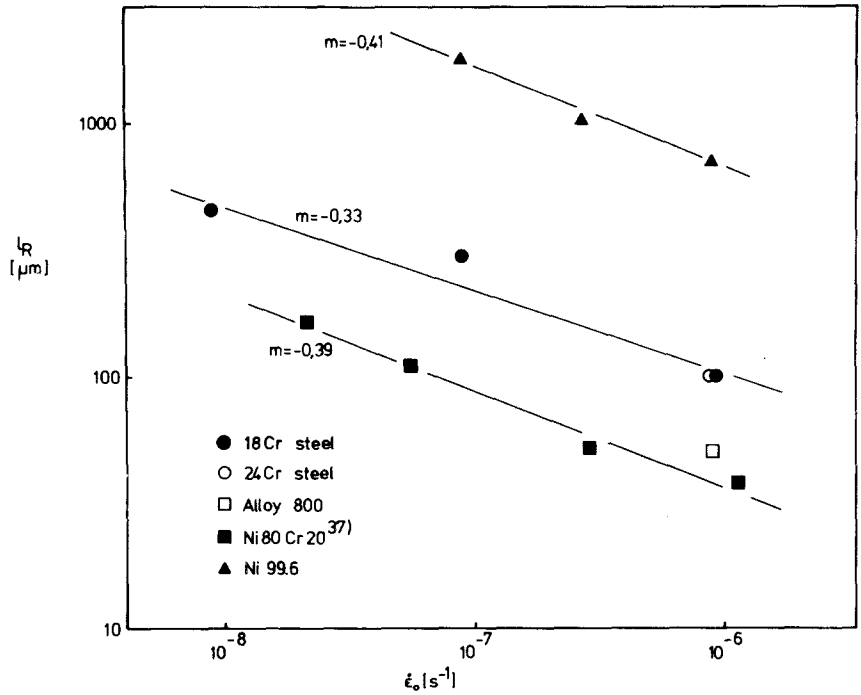

Fig. 6. Mean values of the distances between scale cracks as a function of the applied strain rate.

applied strain rate $\dot{\varepsilon}_o$ (= slope of the dashed line) and the rate of lateral oxide growth $\dot{\varepsilon}_{lat}$ (= slope of the graph $U_{ox} - U_o/U_o$ vs t). The arrow in Fig. 10 divides the graph into two time regions. In the left time region, $\dot{\varepsilon}_{lat}$ exceeds the applied strain rate. Therefore, no tensile stresses are expected in the scale as well as no scale cracking. Cracking is, however, probable in the right time region where the applied strain rate $\dot{\varepsilon}_o$ exceeds the lateral growth rate $\dot{\varepsilon}_{lat}$. An important feature seems to be the decrease of the lateral oxide-growth rate with time. The lateral growth rate has a maximum at an applied strain rate of about $10^{-7}\,s^{-1}$, which indicates that lateral growth can be enhanced by oxide deformation.

In Fig. 8 the value of $\varepsilon_{lat} = (U_{ox} - U_o)/U_o$ for the deformed specimen after 100 hr has become negative because after very large strains (in this case 28%!) the scale-crack faces in the wrinkles have moved far apart from each other (compare Fig. 3). Accordingly, in cross sections also, regions are included in the measurements where the cut has been made between the scale-crack faces. In these regions only the scale which had newly formed on the metal after cracking of the wrinkles is visible in a cross section,

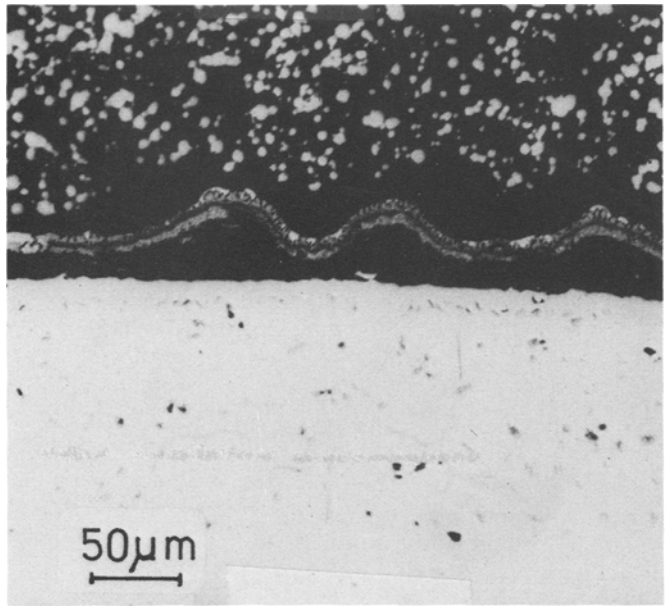

Fig. 7. Example of a wrinkled oxide scale on the 18 Cr steel (metallographic cross section).

whereas the crack faces of the original wrinkles are lying in a plain below the cross section plain. Thereby, a lesser oxide length results from the measurements at very large strains than the one representing lateral oxide growth. This problem only appears for the specimens tested at the highest strain rate of about $10^{-6}\,s^{-1}$ after longer testing times (i.e., high strains); see Fig. 8. At the lower strain rates with lower strains at the end of the tests there are no problems of this kind.

The values from the scale-thickness measurements are shown in Figs. 11 and 12. The values of the ferritic steel with Ce addition reached 1 μm after 100 hr. This was near the lower limit of the optical resolution of the microscope.

The Course of Internal Corrosion

The course of internal corrosion was investigated in metallographic and EPMA examinations. In nondeformed specimens a slight internal oxidation of Al had been found for the ferritic steels (except the 18 Cr-Ce steel) and Alloy 800. Increased internal corrosion had occurred for deformed specimens above certain strains and strain rates in the form of nitridation

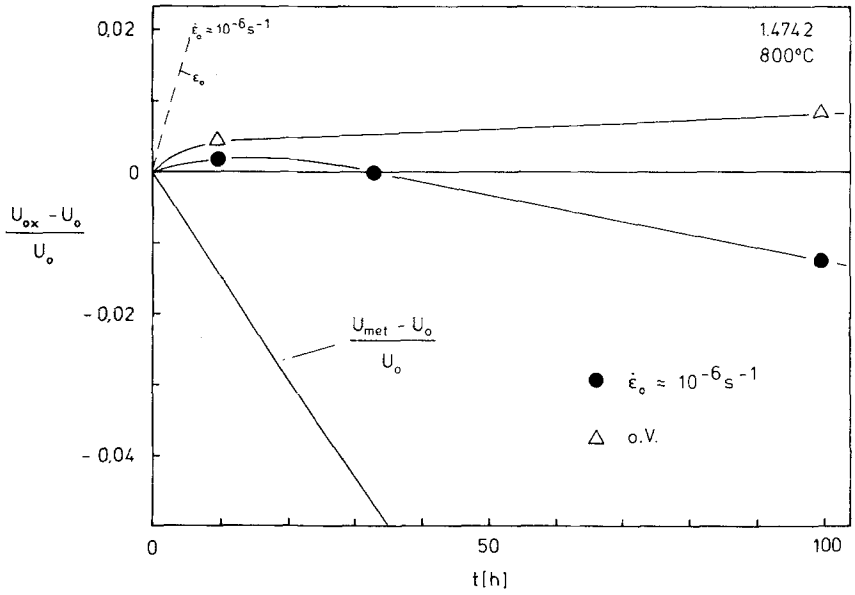

Fig. 8. Lateral-oxide growth on the 18 Cr steel as a function of time for specimens deformed by $\dot{\varepsilon}_o \approx 10^{-6}\ s^{-1}$ and for undeformed specimens (=o.V). U_{ox} = oxide length in circumferential direction; U_o = specimen circumference before the test; U_{met} = circumference of the metal substrate.

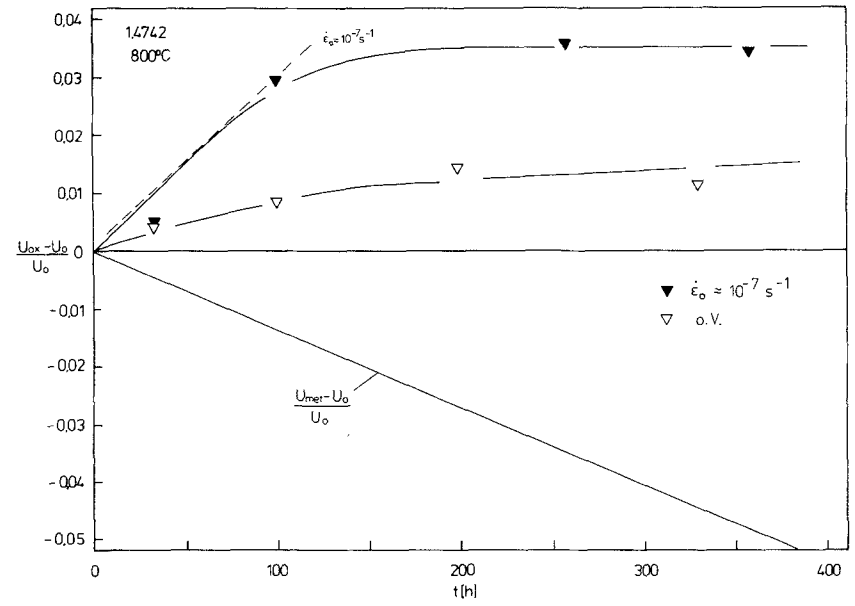

Fig. 9. Lateral-oxide growth on the 18 Cr steel as a function of time for specimens deformed by $\dot{\varepsilon}_o \approx 10^{-7}\ s^{-1}$ and for undeformed specimens (=o.V.). UU_{ox}, U_o, U_{met} as in Fig. 8.

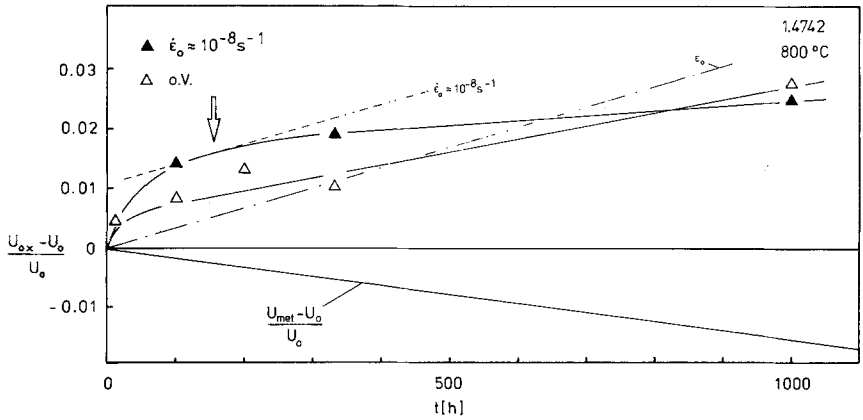

Fig. 10. Lateral-oxide growth on the 18 Cr steel as a function of time for specimens deformed by $\dot{\varepsilon}_o \approx 10^{-8}\ s^{-1}$ and for undeformed specimens (=o.V). U_{ox}, U_o, U_{met} as in Fig. 8.

of Al by nitrogen from air in the ferritic steels (with the exception of the 18 Cr-Ce steel) and in the form of internal oxidation of Al preferentially along metal grain boundaries in Alloy 800. The results of the measurements are shown for the strain rates of 10^{-6} and $10^{-8}\ s^{-1}$ in Fig. 13. A marked difference between the values of deformed and nondeformed specimens is observed after certain testing times for the 18 Cr steel at strain rates from 10^{-6} to $10^{-8}\ s^{-1}$, for the 24 Cr steel at strain rates of 10^{-6} and $10^{-7}\ s^{-1}$, and for Alloy 800 at strain rates of 10^{-6}, 10^{-7}, and to a lesser extent after long testing times at $10^{-8}\ s^{-1}$. No internal corrosion was found in deformed and nondeformed specimens of the 18 Cr-Ce steel under all conditions.

Acoustic Emission Results and Comparison to the Results from Other Methods of Investigation

The principle of the procedure in the work of the present paper is demonstrated by the example in Fig. 14. The upper graph, showing the course of lateral oxide growth as a function of time, indicates that cracking should not be expected at times shorter than indicated by the arrow (approx. 150 hr) since the lateral growth rate $\dot{\varepsilon}_{lat}$ exceeds the applied strain rate at these times. From the results of the acoustic emission measurements (middle graph, Fig. 14, sum of acoustic events vs time), it can be concluded that cracking starts in a time region of 160-310 hr (indicated by the hatched area) and at strains of 0.45-0.95%, respectively. Curve I represents the lower limit and curve II the upper limit of the scatterband for the occurrence of a first strong increase of the sum of acoustic impulses in different tests. The lower graph shows the course of internal corrosion (nitridation) for

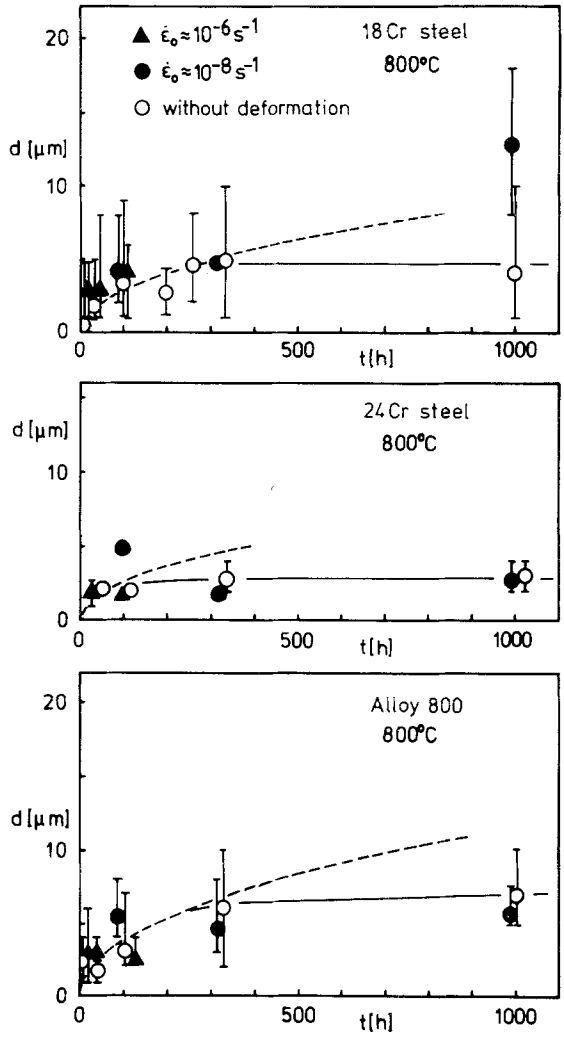

Fig. 11. Oxide-scale thickness as a function of time.

deformed and non-deformed specimens. Up to a testing time of about 200 hr, no severe difference is observed between the values for the depth of internal corrosion of deformed and nondeformed specimens. At longer times (i.e., higher strains), a strong increase in internal corrosion is found for the deformed specimens, whereas the depth of internal corrosion remains constant in nondeformed specimens. (For this example cracking leads to enhanced internal corrosion.)

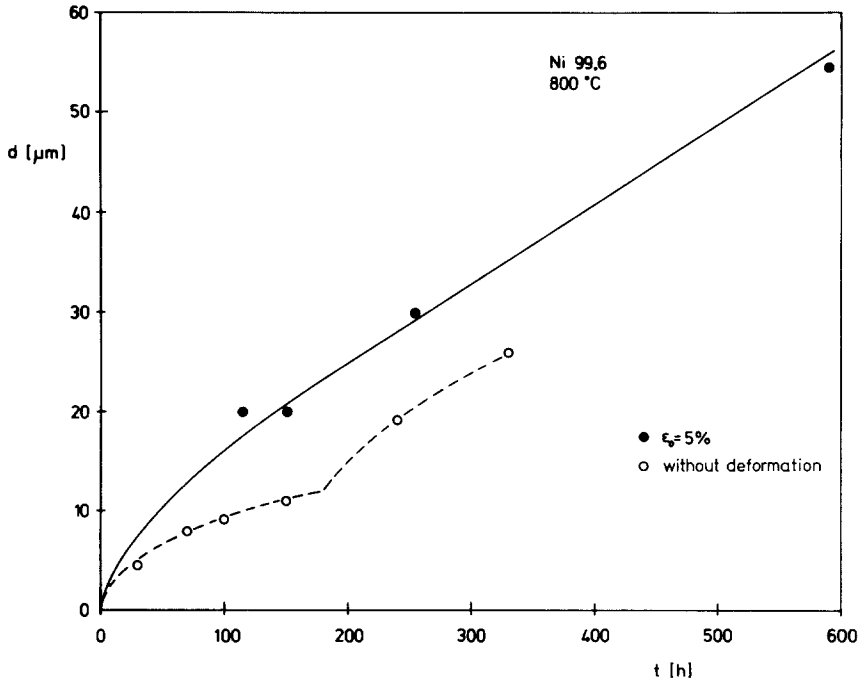

Fig. 12. Oxide scale thickness as a function of time for Ni 99.6.

Additional information is gained from the surface investigations which had revealed scale cracks after certain strains. A summary of all these measured data in graphical form is given in Figs. 15–17. No contradictions exist from the results of these figures. In several cases cracking had occurred, but no increase in internal corrosion was found, which is not a matter of inconsistency but an indication of the healing capabilities of those scales.

Since AE allows an in-situ measurement of the moment of scale cracking during the experiment, and the AE data were supported by the results from the other methods of investigation, the following discussion will be based on the data from AE measurements. These are shown in Fig. 18, where the strains ε_B^{ox} to the beginning of a strong increase in AE activity (i.e., scale cracking) are plotted as a function of the applied strain rates.

The upper graph shows three curves. The black points represent the values from measurements where straining and oxide scale formation started nearly at the same time. The open round symbols are from experiments where the specimens had been strained after a preoxidation time of 330 hr without load. After 330 hr the contribution by lateral growth of the oxide scale has become small because $\dot{\varepsilon}_{lat}$ decreases with time (see Fig. 10). The

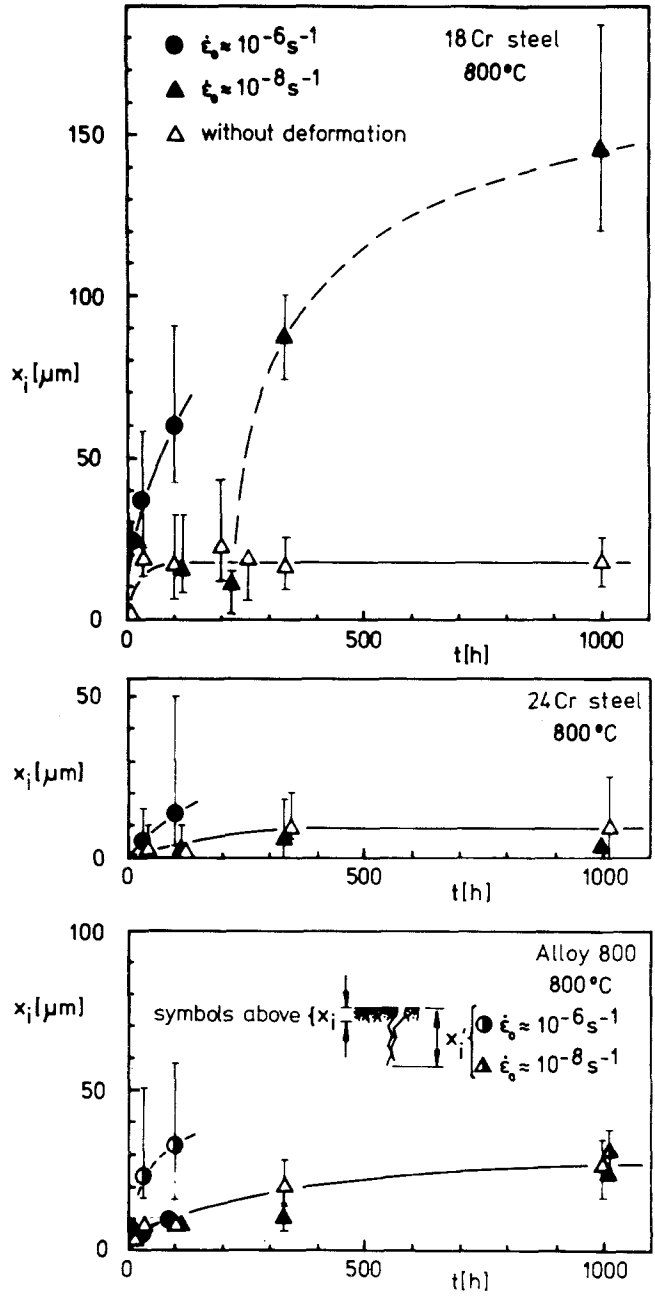

Fig. 13. Depth of internal corrosion as a function of time.

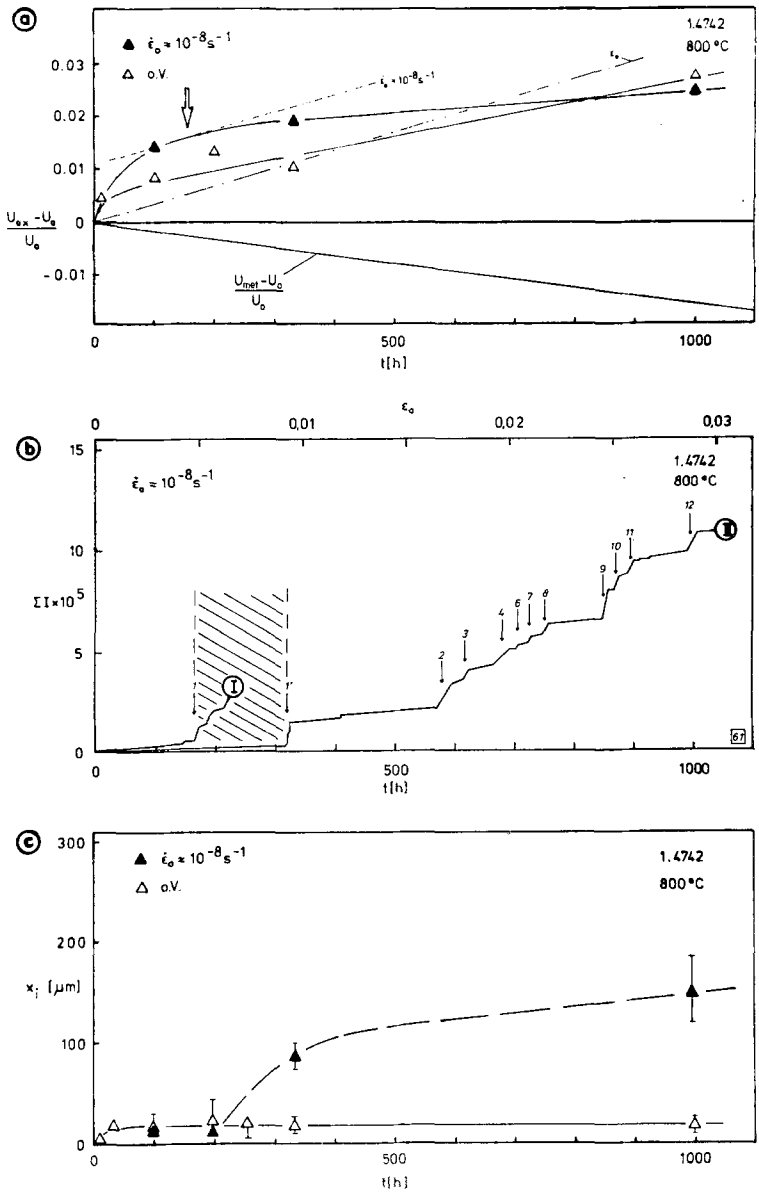

Fig. 14. Lateral-oxide growth, acoustic emission, and internal oxidation interrelationships.

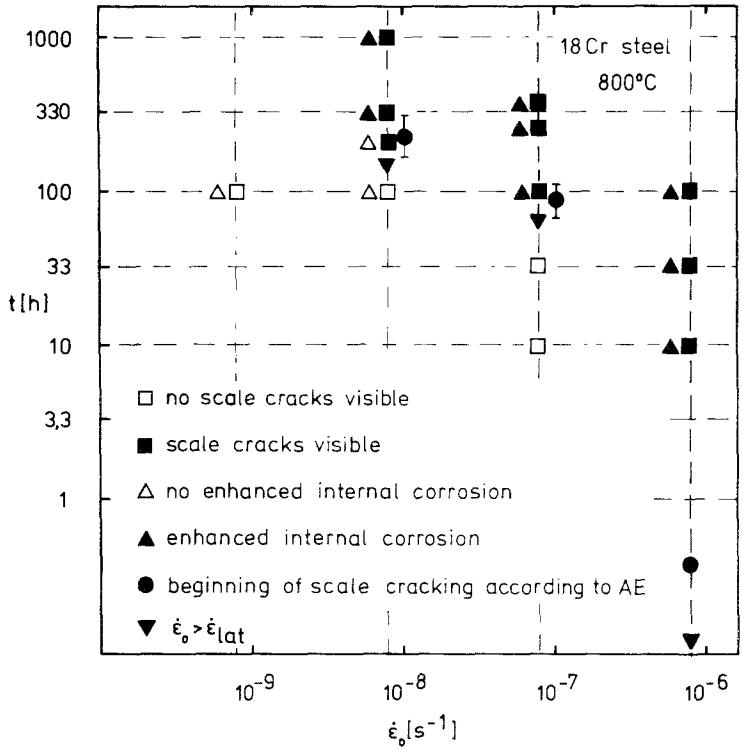

Fig. 15. Summary of the experimental results concerning scale cracking for the 18 Cr steel.

open squares represent the values from the ferritic steel with Ce addition. With the exception of the experiments of Ni 99.6, which included a load-free preoxidation time of 100 hr, and those of the 18 Cr steel with a preoxidation time of 330 hr, all other values in the graphs in Fig. 18 are from experiments where straining and oxide scale formation started nearly at the same time (heating up of the furnaces lasted about 1 hr before the straining tests were begun).

DISCUSSION

Strain-to-Cracking of the Oxide Scales

Possible Models

Natural oxide scales may contain voids and flaws. Therefore, during straining, unequal stress distribution will develop in the scale. Stress

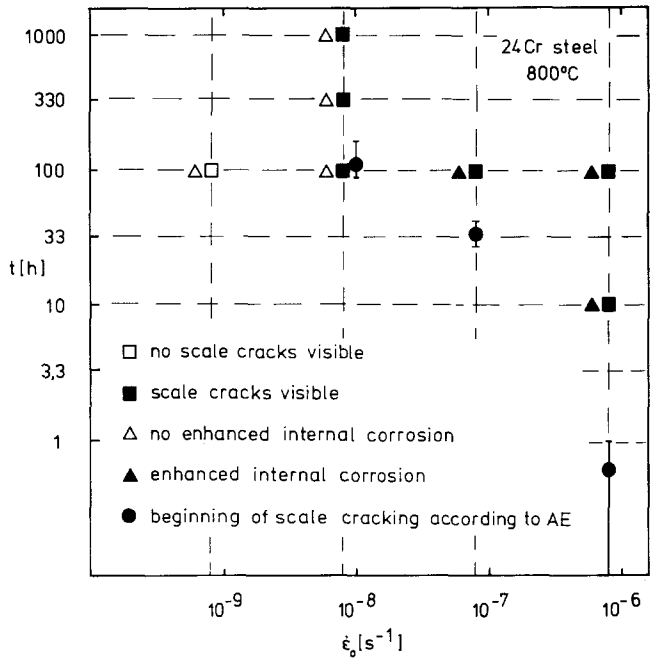

Fig. 16. Summary of the experimental results concerning scale cracking for the 24 Cr steel.

concentrations will arise around these faults according to

$$\sigma_1(x, y, z) = K(x, y, z) \cdot \sigma_m \tag{1}$$

in the case of linear, elastic behavior of the oxide. Here σ_1 = local stress at the site (x, y, z) in a scale with flaws and notches, σ_m = stress in a flaw-free scale of equal thickness, and K = a stress concentration factor depending on flaw length, flaw-tip curvature, and distance from the flaw tip at the site (x, y, z).

The situation in a scale under tensile stress containing flaws is shown schematically in Fig. 19a. Stress peaks exist at the tips of flaws and notches. The σ_1 values in Fig. 19 represent the maximum values in the scale as a function of x, (x = coordinate parallel to the straining direction). Increasing the strain leads to an increase of σ_1 in the oxide. Cracking of the scale starts at sites where σ_1 reaches the critical value σ_c for breaking the bonds in the oxide; Fig. 19b. The stress in the scale is locally released at these sites, whereas, with continuing straining, the stress peaks at other sites and will reach σ_c one after the other so that a crack-formation sequence is initiated in the scale; Fig. 19c.

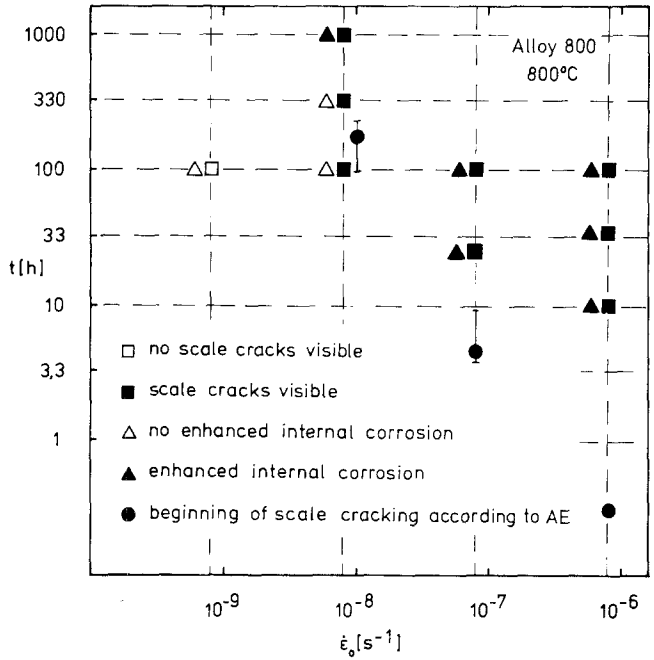

Fig. 17. Summary of the experimental results concerning scale cracking for Alloy 800.

In growing scales a stress gradient across the scale is built up by thickness growth of the oxide if straining and growth occur simultaneously. Oxide-volume elements which had been formed earlier contain higher stresses from straining than elements that were just formed. This is one difference from the behavior of bulk oxides. Another important difference is the potential existence of lateral growth stresses in growing oxide scales on metals. As shown earlier, lateral-oxide growth can be of a considerable amount.

For a precise prediction of the cracking behavior of oxide scales, all these effects should be included in a stress-distribution analysis of the scales. An effective tool for this analysis might be the finite-element method which, however, is not applied in this paper. In the following considerations a finite-volume element in the scale, where the stress has the maximum value σ, is taken for the characterization of the deformation behavior of the oxide scale. This procedure seems to be justified when aiming at the critical values for the beginning of scale cracking, because cracking will start at this site when the stress σ in this element reaches σ_c.

The following reflections are performed to allow a transition from the maximum local stress in the scale, σ (in the finite element considered), to

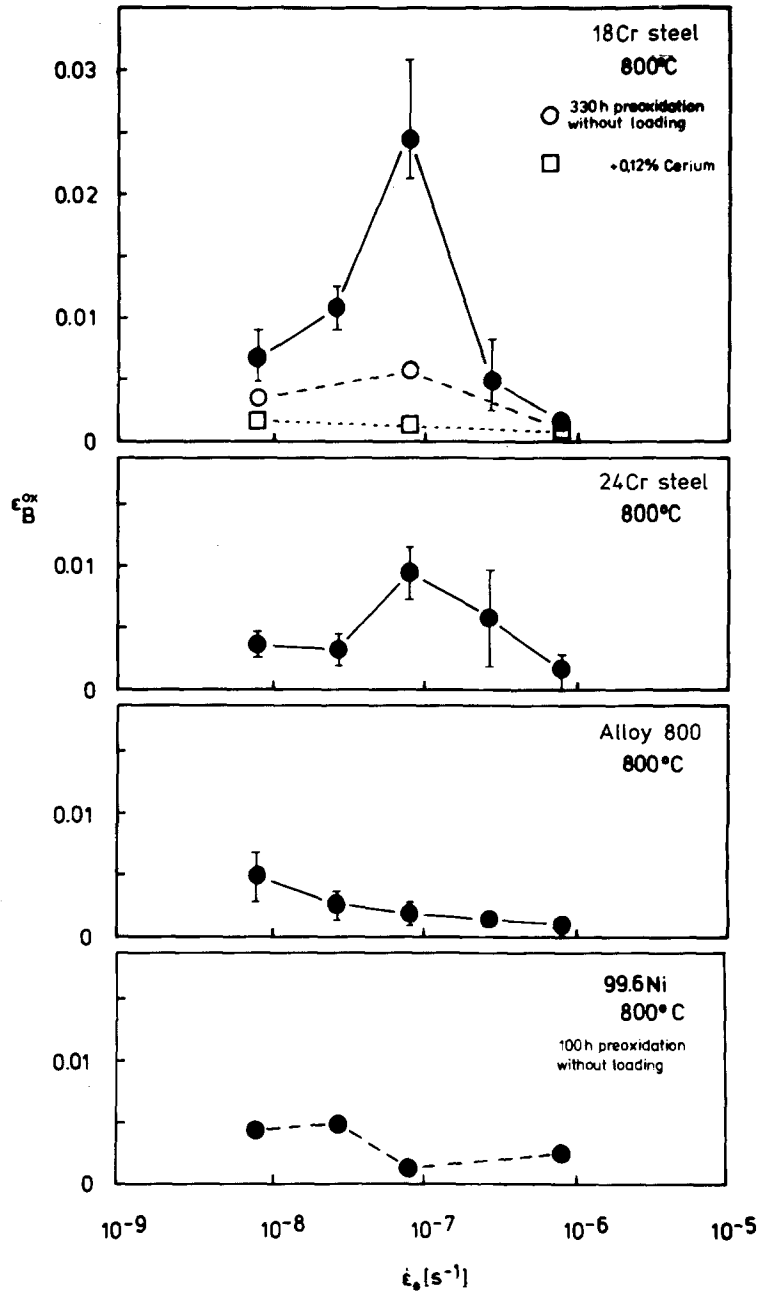

Fig. 18. Strains for the beginning of oxide-scale cracking as a function of the applied strain rate.

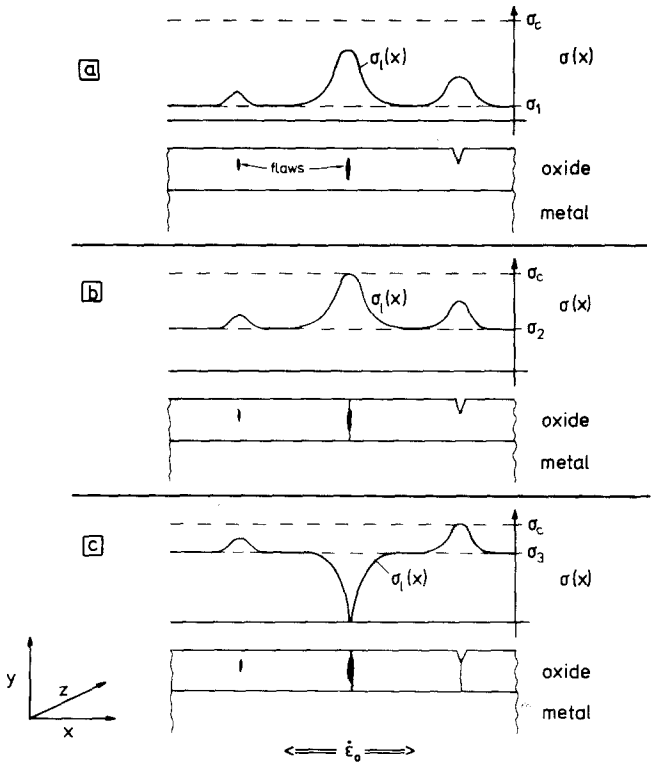

Fig. 19. Schematic representation of the stress distribution in an oxide scale under tensile strain.

parameters like strain and strain rate of the specimen, which can be measured in the expriments. Straining of the metal substrate (and thus of the oxide scale) occurs by a constant strain rate ($\dot{\varepsilon}_o$) corresponding to the situation encountered in the experiments. It is assumed that one or more of the following components contribute to scale deformation: (a) elastic part of deformation, (b) plastic part by creep deformation, and (c) lateral-growth effects. Three possible cases are considered, which are based on model considerations by Riedel.[5]

Case I. Purely elastic behavior of the scale before cracking. This case is expected below the transition temperature for oxide deformation[19] if no diffusional processes (growth processes) affect the deformation behavior of the scale. The scale is deformed elastically by $\dot{\varepsilon}_0 = \dot{\varepsilon}_{el}$ (with $\dot{\varepsilon}_{el}$ being the strain rate of elastic deformation in the scale). The stress, σ, rises proportionally to the elastic strain, ε_{el}, and reaches σ_c at a critical elastic strain value, $\varepsilon_c \cdot \varepsilon_c$ is independent of the applied strain rate and can be used as an experimentally measurable criterion for scale cracking in this case.

Case II. Creep deformation of the scale. Creep deformation is expected above the transition temperature, and in this case elastic deformation will be involved also. Thus, deformation of the oxide by the applied strain rate, $\dot{\varepsilon}_o$, includes two contributions:

$$\dot{\varepsilon}_{el} = \dot{\sigma}/E \qquad \text{elastic part} \tag{2}$$

$$\dot{\varepsilon}_{pl} = B\sigma^n \qquad \text{plastic part by creep} \tag{3}$$

$$\dot{\varepsilon}_o = \dot{\varepsilon}_{el} + \dot{\varepsilon}_{pl} = \dot{\sigma}/E + B\sigma^n \qquad \text{entire scale deformation} \tag{4}$$

B is the creep constant, E is Young's modulus, n is the stress exponent, and $\dot{\sigma}$ is the stress change rate. If stationary creep occurs in the scale, then $\dot{\sigma} = 0$ at constant $\dot{\varepsilon}_o$, and $\dot{\varepsilon}_o = \dot{\varepsilon}_{pl} = B\sigma^n$. This implies that σ does not reach σ_c in the stationary-creep region. Considerable strains to cracking would be expected until creep damage in the oxide increases the local stress concentrations above σ_c and leads to oxide fracture. Increasing the strain rate, $\dot{\varepsilon}_o$, results in an increase of stress, σ (see above). Thus, σ_c can be reached before stationary creep is attained by increasing $\dot{\varepsilon}_o$ to a critical strain rate, $\dot{\varepsilon}_c$. Accordingly, $\dot{\varepsilon}_c$ can be used as a criterion for scale cracking in case II.

Case III. Lateral oxide growth occurring simultaneously during scale deformation. Lateral oxide scale growth would result in an increase in oxide-scale "length" with the rate $\dot{\varepsilon}_{lat}$, if the scales were allowed to move freely. The same length change of the oxide can be achieved by a fictive stress σ_{lat}:

$$\dot{\varepsilon}_{lat} = \dot{\sigma}_{lat}/E + B\sigma_{lat}^n \tag{5}$$

The effective strain rate, $\dot{\varepsilon}$, acting in the scale and determining the stress level, results from the difference

$$\dot{\varepsilon}_o - \dot{\varepsilon}_{lat} = \dot{\varepsilon} = (\dot{\sigma} - \dot{\sigma}_{lat})/E + B(\sigma^n - \sigma_{lat}^n) \tag{6}$$

This means that tensile stresses resulting from straining are reduced by lateral-oxide growth, while compressive stresses from deformation would be increased. Cracking is expected again at σ_c. Applying the criterion from case I (assumed that no creep in the scale occurs) yields

$$\varepsilon = \varepsilon_o - \varepsilon_{lat} = (\sigma - \sigma_{lat})/E < \sigma_c/E = \varepsilon_c$$

or

$$\varepsilon_o < \varepsilon_c + \varepsilon_{lat} \tag{7}$$

where ε is effective strain in the scale, i.e., larger tensile substrate-strains, ε_o, to scale cracking are possible than without lateral growth. Applying the

criterion from case II (stationary creep in the scale) leads to

$$\dot{\varepsilon} = \dot{\varepsilon}_o - \dot{\varepsilon}_{lat} = B(\sigma^n - \sigma_{lat}^n) < B\sigma_c^n = \dot{\varepsilon}_c$$

or

$$\dot{\varepsilon}_o < \dot{\varepsilon}_c + \dot{\varepsilon}_{lat} \tag{8}$$

i.e., larger tensile strain rates, $\dot{\varepsilon}_o$, are possible without scale cracking in the case of lateral growth. Even if $\dot{\varepsilon}_o$ exceeds $\dot{\varepsilon}_c + \dot{\varepsilon}_{lat}$, then the time for scale cracking is retarded according to relation (7), compared to the behavior without lateral growth. As a conclusion from this it follows:

1. Lateral, oxide-scale growth increases the tensile substrate strain to the beginning of scale cracking;
2. In the case where creep deformation occurs, lateral growth may also increase the tolerable tensile strain rate for the oxide scale.

The entire deformation of the oxide scale up to the beginning of scale cracking may contain one or more of the following components:

$$\varepsilon_B^{ox} = \varepsilon_{el} + \varepsilon_{pl} + \varepsilon_{lat} \tag{9}$$

where ε_B^{ox} is the substrate strain for the onset of scale cracking. In the next section an attempt is made to ascertain which of these components contribute to the deformation behavior of the oxide scales investigated in this paper and which of the discussed cases seems to be applicable.

Application of the Models to the Results

In Fig. 18 and in Table II the mean values for the substrate strain for cracking of the oxide scales are shown. Most of these values are comparatively low.

In all cases where deformation of the oxide occurs, an elastic part, ε_{el}, will have a share. The order of magnitude of the elastic strain leading to cracking of bulk Al_2O_3 can be estimated from data in ref. 9. Room-temerature data (in this case the entire deformation to cracking will be purely elastic in nature) as well as data for 800°C, lead to critical tensile strains for cracking of about 0.07%. Since the flaw sizes in sintered bulk Al_2O_3, for which these values were measured, are expected to be larger than in as-grown oxide scales and thus more critical, it can be expected that values of the strain for scale cracking, ε_B^{ox}, of this order of magnitude are an indication of purely elastic scale deformation up to the point of cracking. For the other oxides encountered in the investigated scales, this estimation cannot be performed because the necessary data are lacking. But if one takes the elastic modulus of a predominantly chromia-forming scale[42] and assumes fracture stresses similar to Al_2O_3, the strains for cracking of Cr_2O_3, under the assumption of purely elastic deformation, would amount to about 0.09%.

The same procedure using the elastic modulus for NiO[42] would lead to an elastic fracture strain of the oxide of about 0.07%.

For the 18 Cr and the 24 Cr steel, lateral growth had led to the formation of oxide wrinkles. By this the estimation of ε_{lat} and $\dot{\varepsilon}_{lat}$, respectively, had become possible for the 18 Cr steel. In Fig. 20, it is shown that subtracting $\varepsilon_{\mathrm{lat}}$ at the onset of scale cracking (which is a function of strain rate and can be obtained from Figs. 8–10) from the strain for cracking ε_B^{ox} yields values of the order of magnitude of the elastic strain for cracking of bulk Al_2O_3 (see above) at strain rates of 10^{-6} and $10^{-7}\,s^{-1}$. Therefore, it can be assumed that at these strain rates, the main contributions to the strain for cracking of the oxide scales on the 18 Cr steel were

$$\varepsilon_{el} + \varepsilon_{lat} = \varepsilon_B^{ox} \tag{10}$$

Since the difference $\varepsilon_o - \varepsilon_{lat}$ has a clearly higher value at $\dot{\varepsilon}_o = 10^{-8}\,s^{-1}$ than at the higher strain rates, and the elastic contribution ε_{el} should be independent of strain rate, it may be concluded that at lower strain rates a contribution, ε_{pl} by creep will occur also:

$$\varepsilon_{el} + \varepsilon_{pl} + \varepsilon_{lat} = \varepsilon_B^{ox} \tag{9}$$

This seems to be plausible, since with decreasing strain rate, the probability of a contribution to oxide deformation by diffusional creep increases. The role of lateral growth for scale deformation also becomes obvious when comparing the ε_B^{ox} values from specimens of the 18 Cr steel which had been

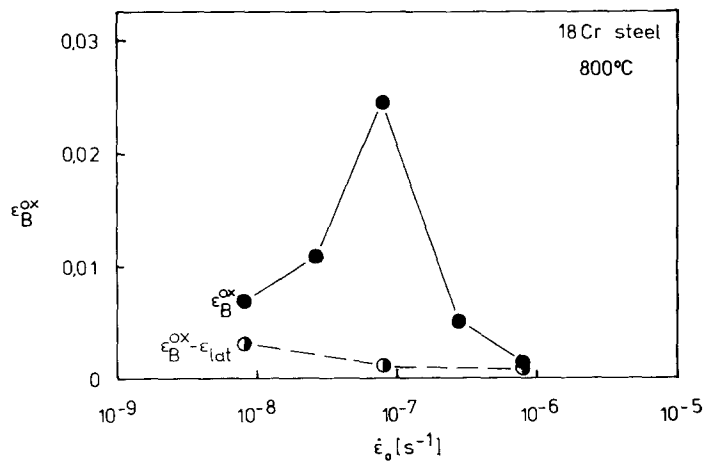

Fig. 20. Fracture strain of the oxide scale on 18 Cr steel with lateral growth (ε_B^{ox}) and after subtracting the contribution by lateral scale growth ($\varepsilon_B^{ox} - \varepsilon_{lat}$). For details see text.

preoxidized for 330 hr with those without preoxidation; Fig. 18. The strains to scale cracking are clearly lower for the preoxidized specimens on which the lateral oxide growth rate had become small compared to the beginning of oxidation (see Fig. 10).

In oxide scales which do not form wrinkles, lateral stresses from growth processes may arise also. This had been observed for NiO scales on pure nickel, where the stresses led to a length increase of the metallic substrate of up to 0.2% at 1000°C.[26]

Table II summarizes which of the contributions ε_{el}, ε_{pl}, and ε_{lat} play a role during straining of the investigated oxide scales on the different

Table II. Deformation Behavior of the Scales[a]

	ε_B^{ox} (%)	ε_{el}	ε_{pl}	ε_{lat}	Case
$\dot{\varepsilon}_o = 1 \times 10^{-6}\,s^{-1}$					
18 Cr steel	0.15	+	−	+	III
18 Cr-Ce steel	0.08	+	−	−	I
24 Cr steel	0.17	+	−	+	III
Alloy 800	0.09	+	−	−	I
Ni 99.6	0.25	+	(+)	(+)	(II,III)
$\dot{\varepsilon}_o = 3 \times 10^{-7}\,s^{-1}$					
18 Cr steel	0.50	+	−	+	III
24 Cr steel	0.57	+	−	+	III
Alloy 800	0.15	+	+	−	II
$\dot{\varepsilon}_o = 1 \times 10^{-7}\,s^{-1}$					
18 Cr steel	2.45	+	−	+	III
18 Cr-Ce steel	0.15	+	+	−	II
24 Cr steel	0.95	+	−	+	III
Alloy 800	0.17	+	+	−	II
Ni 99.6	0.13	+	(+)	(+)	(II,III)
$\dot{\varepsilon}_o = 3 \times 10^{-8}\,s^{-1}$					
18 Cr steel	1.08	+	(+)	+	III
24 Cr steel	0.31	+	(+)	+	III
Alloy 800	0.26	+	+	−	II
Ni 99.6	0.48	+	+	(+)	II (III)
$\dot{\varepsilon}_o = 1 \times 10^{-8}\,s^{-1}$					
18 Cr steel	0.68	+	+	+	III
18 Cr-Ce steel	0.16	+	+	−	II
24 Cr steel	0.37	+	+	+	III
Alloy 800	0.50	+	+	−	II
Ni 99.6	0.44	+	+	(+)	II (III)

[a] For explanation of symbols, see text.

substrate materials at different strain rates. The + sign indicates that a contribution of this part is obvious, the − sign that no mentionable contribution is expected. In case of uncertainty the signs are in parentheses. ε_{lat} has been considered only as an obvious contribution if oxide scale wrinkles had been observed. Possible lateral stresses in the NiO scale according to the observations of Rhines and Wolf[26] are indicated by (+). If a difference remains after subtracting the elastic strain and the contribution of lateral growth from the overall strain to scale cracking, this has been attributed to plastic creep deformation.

The general tendency in Table II is that first, for the scales on Alloy 800 and on the ferritic 18 Cr-Ce steel, cracking occurs after purely elastic deformation at $\dot{\varepsilon}_o = 10^{-6}$ while an increasing plastic contribution from presumably diffusional creep is observed with decreasing strain rates. Second, for the scales on the ferritic 18 Cr and 24 Cr steels, lateral oxide scale growth contributes to deformation (with a maximum at around $\dot{\varepsilon}_o = 10^{-7}\,s^{-1}$) and thus increases the tensile strain to cracking. With decreasing strain rate, the plastic contribution increases also in this case. Third, for the scales on Ni 99.6 it may be possible that there is a contribution from lateral stresses at the strain rates utilized. Again, the contribution from plastic deformation (by diffusional creep) is expected to increase with decreasing strain rates. In the investigated strain-rate region, stationary creep of the oxide does not seem to occur at 800°C, because the contribution ε_{pl} was always very small.

Based on these results the deformation behavior of the oxide scales is assigned to the respective model case of the preceding section (last column in Table II). A general schematic representation of the possible different contributions up to the moment of scale cracking as a function of strain rate is shown in Fig. 21.

Crack Distribution in the Oxide Scales

The crack distribution in the scales may be interesting for various reasons. Scale cracks are sites of increased probability for the beginning of enhanced internal corrosion which may end up in the form of damage to the whole structural part. Numerical values from scale-crack distance measurements are needed for the model-oriented estimation of the crack-healing rate of scales.[39]

The mean values of the distances between the scale cracks are shown in Fig. 6 as a function of the applied strain rate. All results except those from experiments with Ni80Cr20 (ref. 37) come from experiments performed in air where rehealing of scale cracks is not suppressed. The results of measurements on Ni80Cr20 (ref. 37) are from experiments in argon atmos-

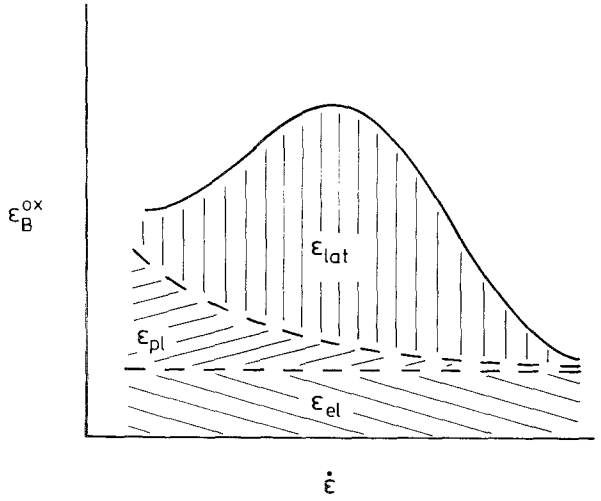

Fig. 21. Schematic representation of the possible contributions to scale deformation as a function of strain rate.

phere after preoxidation in which oxide-growth rates (and thus crack-healing rates) should be close to zero.

Riedel[5] has developed a model which leads to the following relation for the distance l_R between the scale cracks:

$$l_R \propto (d/\dot{\varepsilon}_o)^{1/2} \tag{11}$$

where d is oxide-scale thickness. This relation is based on the assumption that linear, viscous slide of the oxide-scale segments produced by cracking occurs on the substrate metal. Here l_R represents the crack distance at a saturation strain when no further crack formation is expected since the stresses transferred from the substrate strained by $\dot{\varepsilon}_o$ into the scale will not reach σ_c any more. According to the above equation a model-oriented plot of $l_R/\sqrt{d}$ vs. $\dot{\varepsilon}_o$ should lead to a straight line with a slope of -0.5. In Fig. 22 the results were plotted in this way.

Least-square fit lines were calculated, and the values of the slope m of these lines are shown in Fig. 22. (For the results from Ni80Cr20, ref. 37, the value of the lowest investigated strain rate had not been included for these calculations. Least-square fit lines had also been drawn in Fig. 6.) The m value of -0.44 from the results of the scales on Ni 99.6 is close to the predicted value of -0.5. In the other cases m amounts to -0.26 and -0.27.

It would have been surprising if the m values from these measurements had met -0.5 in all cases. There are various reasons to assume that relation (11) cannot be supported by the investigations of this paper. First, with the

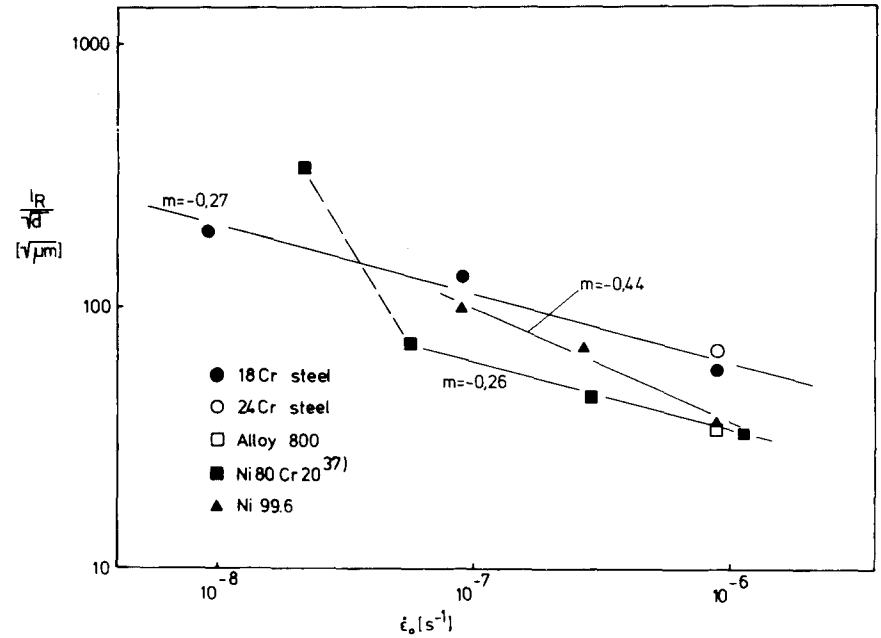

Fig. 22. Model-oriented plot of the distances between scale cracks vs the applied strain rate.

exception of the results from Ni80Cr20 (ref. 37), all experiments had been performed in air, in which cracking-healing processes will lead to conditions not considered by Riedel. Second, $m = -0.5$ represents the case of linear, viscous sliding only. Nonlinear, viscous sliding of the oxide-scale segments results in a lesser strain rate dependence of 1_R than by an exponent of -0.5.[5] Third, in cases of lateral-oxide growth, wrinkle formation had led to a local detachment of the oxide scales with the extent of detachment being a function of time. Therefore, viscous sliding of the oxide on the metal substrate may occur only at adherent sites, the dimensions of which decrease with time. Local scale detachment may also be a result of straining the substrate.[37,43] In this case scale detachment starting from through-scale cracks can be made responsible for the existence of a saturation strain at which no further decrease of l_R occurs.[43] These effects are not included in the model.

Problems may arise with the saturation strain. This seems to be reached after a substrate strain of 4–5%. At the higher strain rates, i.e., around $10^{-6}\,s^{-1}$, this value could be taken out of the experiments. For Ni 99.6 the total strain in the experiments always amounted to 5%, so that the saturation strain should be reached in all cases. The strain values in the experiments

investigating the scales on the other materials were less than 5% at the lower strain rates in some cases. For these cases, the l_R values may decrease further if one increases the strain.

In principle, there is a less marked strain-rate dependence of the l_R values for the scales on the investigated alloys than for the scale on Ni 99.6. Berchtold *et al.*[43] even assume for the scales on Ni80Cr20 that above a strain rate of about $3 \times 10^{-8}\ s^{-1}$ there is no strain-rate dependence of l_R at all if the saturation strain is reached. They attribute such a behavior to the release of stresses in a purely elastically deformed scale by detachment starting at cracks without involving any time-dependent processes (and not by viscous sliding processes at the interface). It is doubted that this conclusion applies to the results from this work. The scales on Ni 99.6 and on Alloy 800 were well adherent at all sites after cracking, and the local scale detachment on the 18 Cr and the 24 Cr steel was mainly a consequence of wrinkle formation by lateral-oxide growth. As shown in Fig. 23 for the example of a scale on Alloy 800, the scale-crack faces have moved apart, although there is a good contact between metal and oxide scale in the neighborhood of the cracks. This allows the assumption that stress relaxation in the scale has occurred via creep at the interface oxide/metal (i.e., linear or nonlinear, viscous sliding).

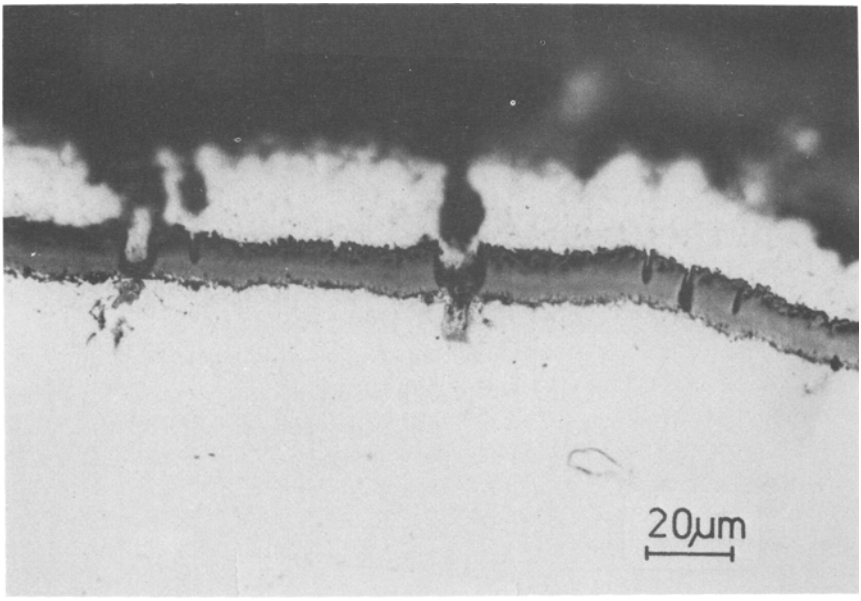

Fig. 23. Example of an adherent, cracked oxide scale on Alloy 800.

The conclusions that can be drawn from the observed crack distributions in the scales are the following. First, according to Riedel's model, linear viscous sliding at the metal/oxide interface leads to the highest strain-rate dependence. Thus, it is assumed that this represents an upper borderline case. Second, no strain-rate dependence is expected if the scale behaves fully elastically and the saturation strain is the consequence of scale detachment starting from through-scale cracks without involving any time-dependent processes. This will be the other borderline case. Third, the observed behavior of the scales ranges between these two borderline cases. This may be due to nonlinear, viscous sliding at the interface, local scale detachment by lateral-growth processes, and/or crack-healing processes in air. Extended scale detachment by straining (with l_R being independent of the strain rate) had not been found in the experiments. If one l_R value at the saturation strain is known from the experiments the two borderlines can be drawn. Provided that scale cracking occurs at lower strain rates, the l_R values at the saturation strain should lie between these two borderlines.

CONCLUSIONS

1. The substrate strains to initiate cracking of the oxide scales on the investigated heat-resistant steels and on Ni 99.6 at 800°C are comparatively low and dependent on strain rate. In detail, the critical-strain values amount to 0.15–2.45% for the 18 Cr steel, 0.08–0.16% for the 18 Cr–Ce steel, 0.17–0.95% for the 24Cr steel, 0.09–0.50% for Alloy 800, and 0.13–0.48% for Ni 99.6.

2. The deformation behavior of the oxide scales under tensile strain can be described in model considerations by three contributions: (a) elastic contribution to deformation, (b) plastic contribution to deformation (presumably mainly by diffusional creep in the oxide), and (c) contribution from lateral-oxide growth effects. In the investigated scales the plastic contribution is rather small at 800°C, whereas lateral-growth effects may increase the strain for scale cracking considerably.

3. The saturation, oxide-scale crack distribution (i.e., the distance between the cracks) may be dependent on the substrate strain rate if time dependent stress relief in the oxide scale, e.g., by viscous sliding of the oxide segments on the substrate metal, occurs. The crack distribution in the NiO scale comes close to the predicted behavior according to the model by Riedel[5] for linear, viscous sliding:

$$l_R \propto (d/\dot{\varepsilon}_o)^{1/2} \tag{11}$$

For the oxide scales on the heat-resistant steels there is a lesser strain-rate dependence of the crack distance l_R. A lesser strain-rate dependence may

be a consequence of (a) nonlinear, viscous sliding; (b) of simultaneous healing processes in the scale; and/or (c) of considerable scale detachment. No strain-rate dependence is expected if stress relief in the scales occurs only via scale detachment starting at through-scale cracks.[43]

4. If one value of l_R at the saturation strain is known for a certain strain rate from experiments, two borderlines can be drawn representing the range of values for l_R expected. The upper line results from a strain-rate dependence of -0.5. The lower line represents strain-rate independence.

5. It has to be taken into account that strains in structural components under service conditions may be larger than the critical strains for scale cracking from these measurements even in the case of proper design. It is, therefore, concluded that cracking of oxide scales cannot be excluded during service. This need not lead to enhanced internal or external corrosion as long as the material possesses a sufficient crack-healing capability.

ACKNOWLEDGMENTS

The author most gratefully acknowledges the helpful discussions with Prof. Rahmel and his assistance by reading critically through the manuscript. Thanks are expressed to all members of Dechema-Institut who contributed to this work with their skillful technical assistance. The work had been financially supported by the Deutsche Forschungsgemeinschaft.

REFERENCES

1. A. Rahmel, ed., *Aufbau von Oxidschichten auf Hochtemperaturwerkstoffen und ihre technische Bedeutung* (Deutsche Gesellschaft für Metallkunde, Oberursel, 1983).
2. M. I. Manning, in Ref. 1, p. 283.
3. M. I. Manning, in *Corrosion and Mechanical Stress at High Temperatures* (Applied Science Publishers, London, 1981), p. 323.
4. J. Armitt, D. R. Holmes, M. I. Manning, D. B. Meadowcroft, and E. Metcalfe, The spalling of steam grown oxide from superheater and reheater tube steels. EPRI Report FP 686 (1978).
5. H. Riedel, *Metal Sci.* **16**, 569 (1982).
6. J. C. Grosskreutz, *J. Electrochem. Soc.* **116**, 1232 (1969).
7. H. E. Evans and R. C. Lobb, *Corr. Sci.* **24**, 209 (1984).
8. A. G. Evans, G. B. Crumley, and R. E. Demaray, *Oxid. Met.* **20**, 193 (1983).
9. G. V. Samsonow, ed., *The Oxide Handbook* (IFI/Plenum, New York, 1973).
10. R. M. Cannon, W. H. Rhodes, and A. H. Heuer, *J. Am. Ceramic Soc.* **63**, 46 (1980).
11. A. H. Heuer, N. J. Tighe, and R. M. Cannon, *J. Am. Ceramic Soc.* **63**, 53 (1980).
12. R. M. Spriggs and T. Vasilos, *J. Am. Ceramic Soc.* **47**, 47 (1964).
13. C. K. L. Davies, *Phys. Metall. React. Fuel Elem.* (Metals Society, London, 1975).
14. L. D. Hou, S. K. Tiku, H. Wang, and F. A. Kroeger, *J. Mat. Sci.* **14**, 1877 (1979).
15. P. A. Lessing and R. S. Gordon, *J. Mat. Sci.* **12**, 2291 (1977).
16. R. W. Cannon and O. D. Sherby, *J. Am. Ceramic Soc.* **60**, 44 (1977).
17. B. J. Dalgleish, A. Fakhr, P. L. Pratt, and R. D. Rowlings, *J. Mat. Sci.* **14**, 2605 (1979).
18. T. G. Langdon, *Metal Forum* **1**, 59 (1978).

19. G. W. Groves, *Proc. Br. Ceramic Soc.* **15**, 103 (1970).
20. R.v. Mises, *Z. angew. Math. Mech.* **8**, 161 (1928).
21. A. G. Evans, *Proc. Br. Ceramic Soc.* **15**, 113 (1970).
22. C. Gandhi and M. F. Ashby, *Acta Met.* **27**, 1565 (1979).
23. B. Burton and G. L. Reynolds, *J. Mat. Sci.* **13**, 219 (1978).
24. K. N. Strafford and G. Smith, *Oxid. Met.* **14**, 119 (1980).
25. J. Cabrera-Cano and J. Castaing, *J. Phys. Lett.* **41**, 119 (1980).
26. F. N. Rhines and J. S. Wolf, *Met. Trans.* **1**, 1701 (1970).
27. M. J. Bennett and J. B. Price, *Metallic Corrosion II* (DECHEMA, Frankfurt, 1981), p. 1026.
28. K. P. Lillerud and P. Kofstad, *J. Electrochem. Soc.* **127**, 2397 (1980).
29. P. Kofstad and K. P. Lillerud, *J. Electrochem. Soc.* **127**, 2140 (1980).
30. M. Schütze and A. Rahmel, *Corrosion Resistant Materials for Coal Conversion Systems* (Applied Science Publishers, London, 1983), p. 439.
31. K.-H. Döhle, A. Rahmel, M. Schmidt, and M. Schütze, in Ref. 3, p. 441.
32. J. Barbehön, K.-H. Döhle, and M. Schütze, *Computer Appl. Lab.* **5**, 336 (1984).
33. F. A. Golightly, F. H. Stott, and G. C. Wood, *Oxid. Met.* **10**, 163 (1976).
34. F. A. Golightly, G. C. Wood, and F. H. Stott, *Oxid. Met.* **14**, 217 (1980).
35. R. G. Miner and V. Nagarajan, *Oxid. Met.* **16**, 313 (1981).
36. D. Caplan and G. I. Sproule, *Oxid. Met.* **9**, 459 (1975).
37. M. Welker, Diploma Thesis, University of Erlangen-Nürnberg (1983).
38. M. Schütze and A. Rahmel, *High Temperature Corrosion* (NACE, Houston, 1983), p. 421.
39. M. Schütze and A. Rahmel, in Ref. 1, p. 245.
40. C. Coddet, G. de Barros, and G. Beranger, in Ref. 3, p. 417.
41. G. de Barros, G. Beranger, J. F. Chretien, and C. Coddet, Action concertée Metallurgie, Université Technologie de Compiegne (1980).
42. R. C. Hurst and P. Hancock, *Korr.* **24**, 33 (1973).
43. L. Berchtold, M. Welker, and H. G. Sockel, *Werkstoffe Korr.*, to appear.